Electronic Supplementary Material (ESI) for Biomaterials Science.

Electronic Supporting Information (ESI)

Melatonin/Polydopamine Nanostructures for Collective Neuroprotection based Parkinson's Disease Therapy

Anup K. Srivastava, Subhasree Roy Choudhury, Surajit Karmakar**

Institute of Nano Science and Technology, Mohali, Punjab, India

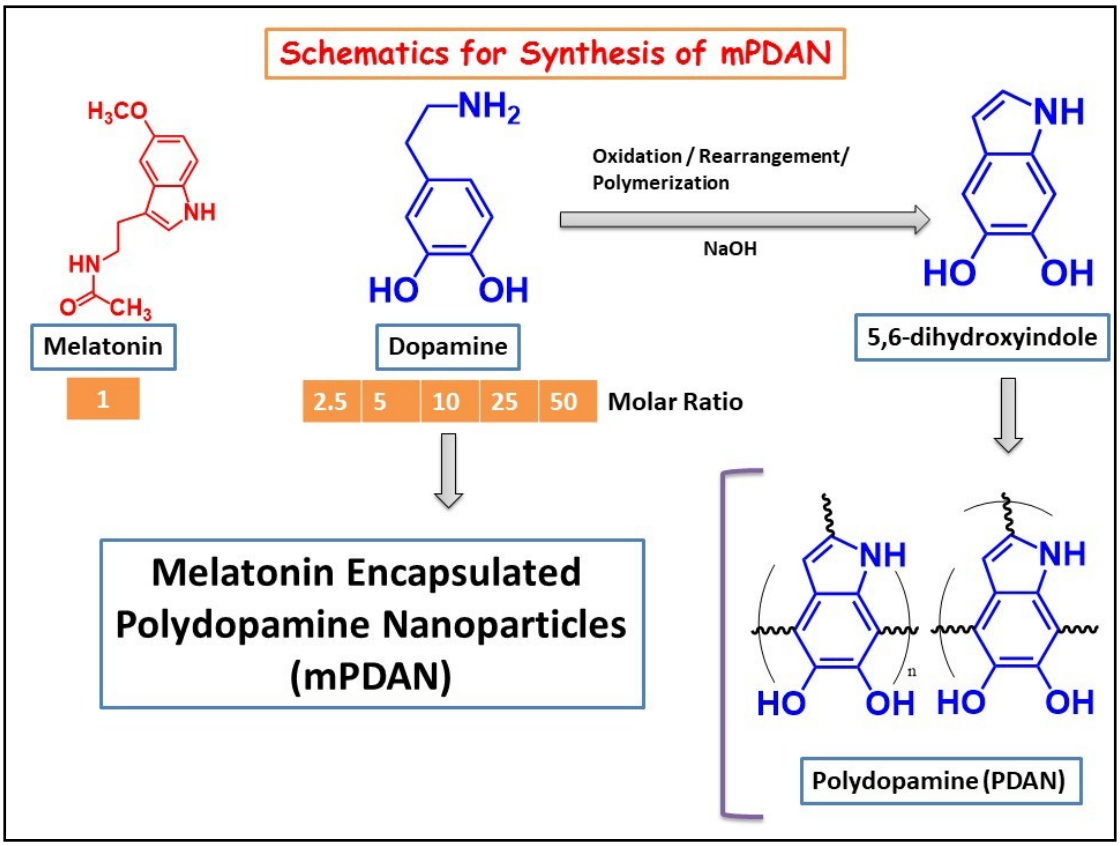

Figure S1. The representative schematics outline the preparation of mPDAN, the variable dopamine/melatonin ratio (2.5, 5, 10, 25, and 50) are determining the physicochemical characteristics, Mel loading, and release behavior. The melatonin enriched polydopamine nanoformulation are prepared by following mild oxidation assisted self-assembly of the DA.

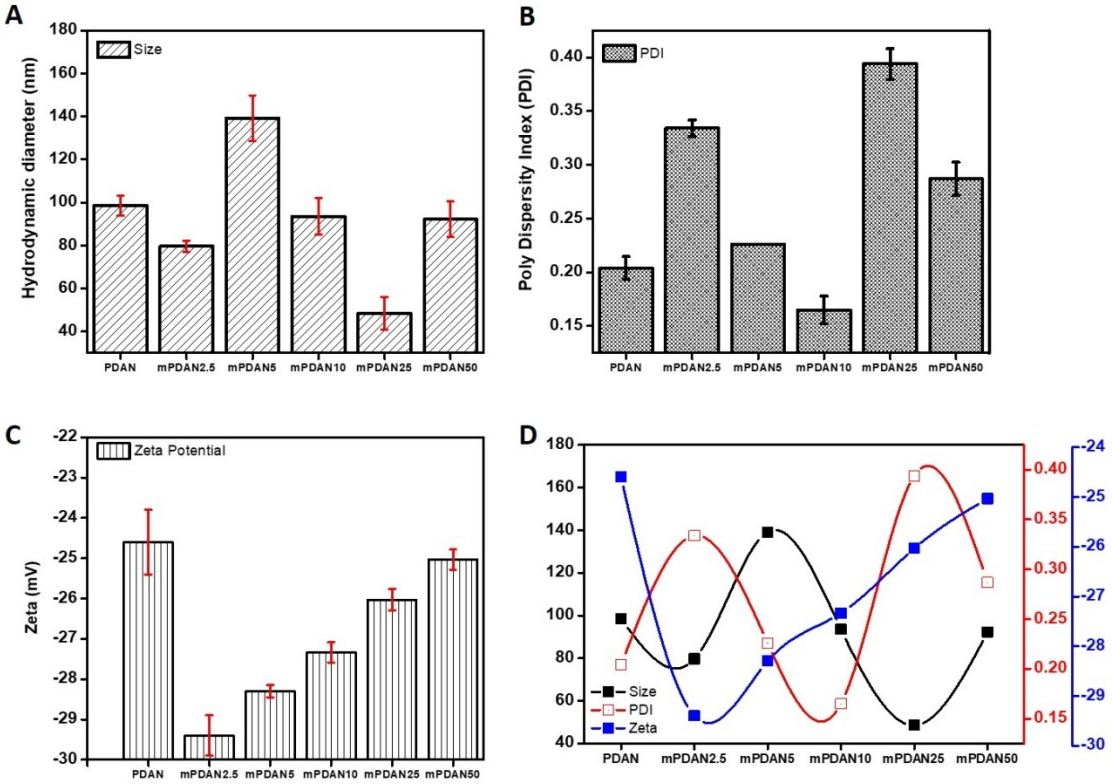

Figure S2. The variable-ratio of DA/Mel (2.5,5,10,25 and 50) produced the mPDAN, abbreviated as mPDAN2.5, mPDAN5, mPDAN10, mPDAN25 and mPDAN50 along with placebo PDAN nanostructures without Mel; (A) The hydrodynamic diameter obtained by dynamic light scattering (DLS); (B) The polydispersity index (PDI) of the obtained nanostructures; (C) The zeta potential change reveal the Mel interaction and loading in mPDAN; (D) The composite diagram representing the hydrodynamic diameter, PDI and Zeta potential of the obtained mPDAN variants.

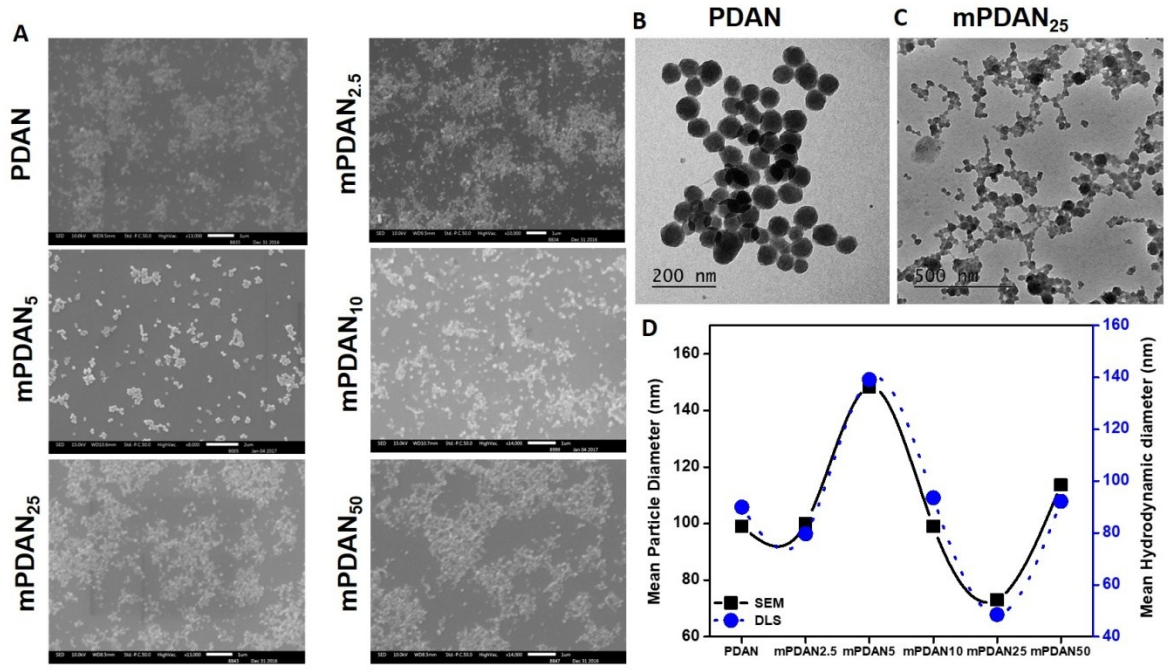

Figure S3. The morphological assessment of mPDAN variants prepared by considering variable ratio of DA/Mel (2.5,5,10,25 and 50) and abbreviated as mPDAN2.5, mPDAN5, mPDAN10, mPDAN25 and mPDAN50 along with placebo PDAN nanostructures without Mel; (A) The Scanning electron micrograph (SEM) of the mPDAN variants, scale bar = 1 µm and 2 µm ; (B and C) The Transmission electron microscopic (TEM) image of the PDAN and mPDAN2.5, scale bar = 200 nm and 500 nm; (D) The comparison of the hydrodynamic diameter obtained from DLS and mean particle diameter observed under SEM, show similarity in the particles diameter.

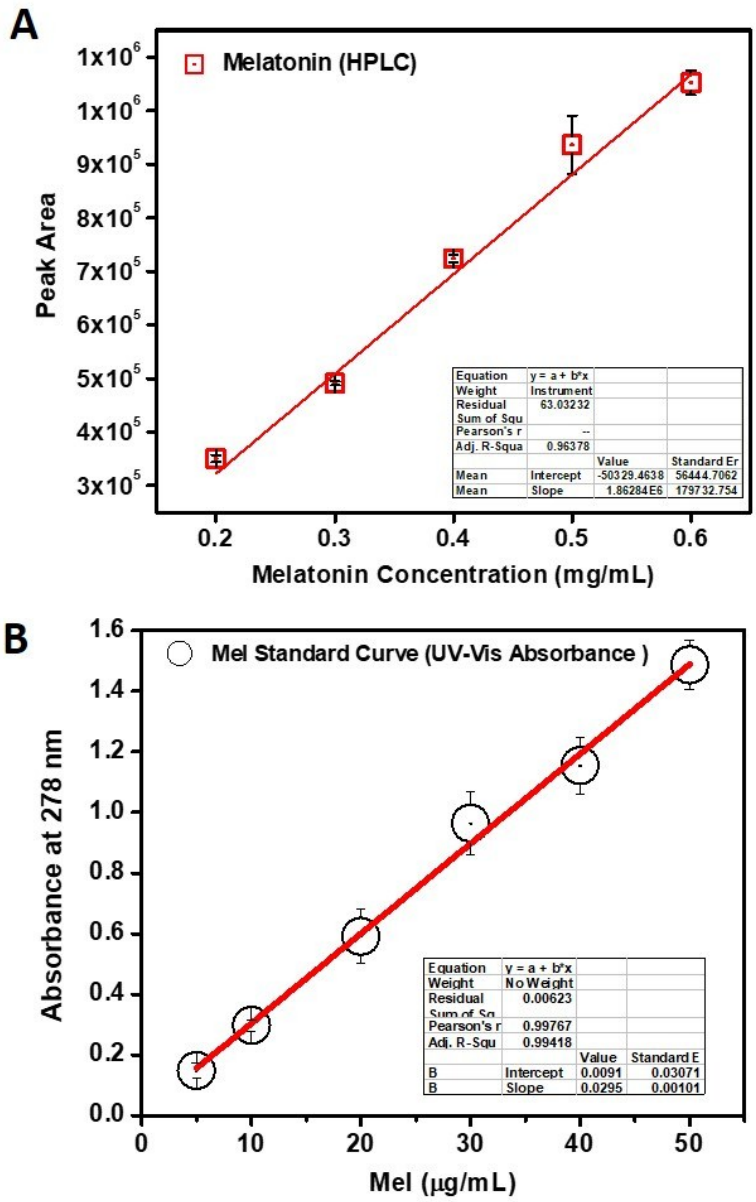

Figure S4. The standard curve was plotted for estimation of effective Mel loading, and release. (A) the standard curve obtained by linear regression analysis of the plot constructed by the integrated curve area of the melatonin from 0.2 mg mL^{-1} to 0.6 mg/mL^{-1} using high-performance liquid chromatography. (B) The UV-Vis absorbance of the Mel from 5 μg mL^{-1} to 50 μg mL^{-1} were plotted and fitted by linear regression analysis. The R^2 value of the fits is> 0.95 used for the estimation of Mel loading and release at different time point.

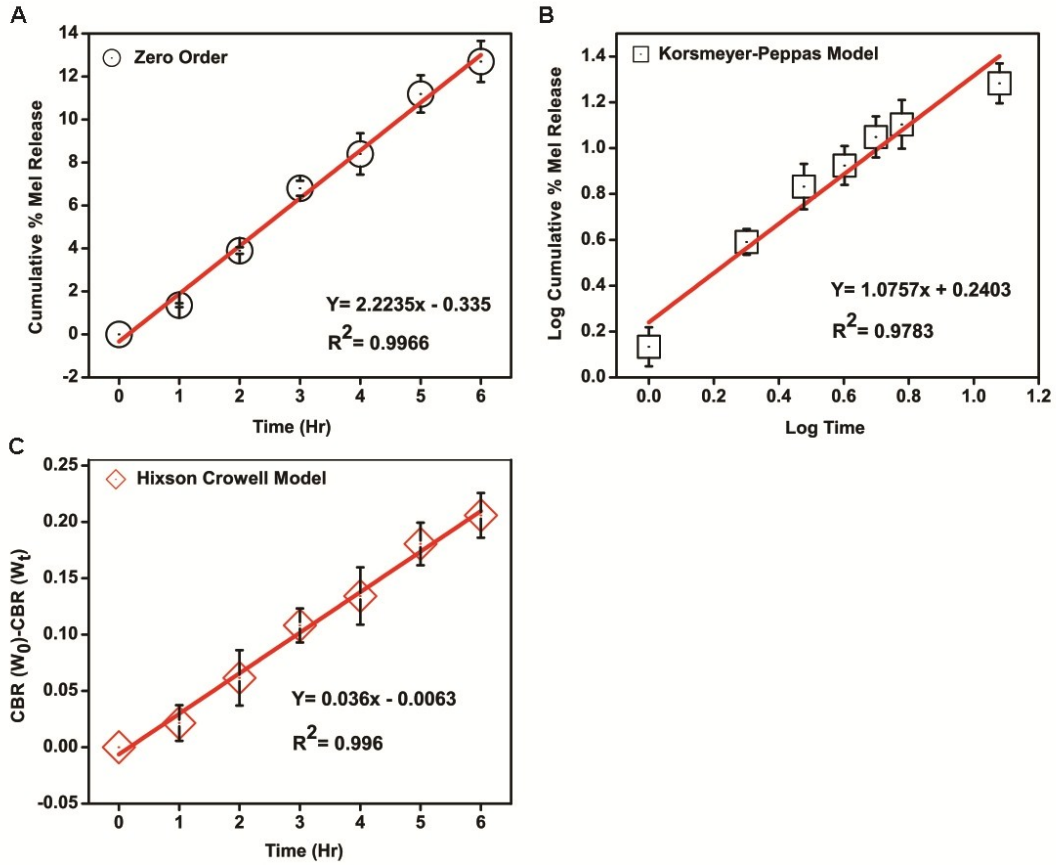

Figure S5. The kinetic analysis of the Mel release data fitted to (A) zero-order kinetics (R^2 = 0.996), (B) Korsmeyer-Peppas model (R^2 = 0.978) (C) Hixson Crowell Model model (R^2 = 0.996). The concentration-independent, sustained Mel release following anomalous diffusion transport were elucidated form the results.

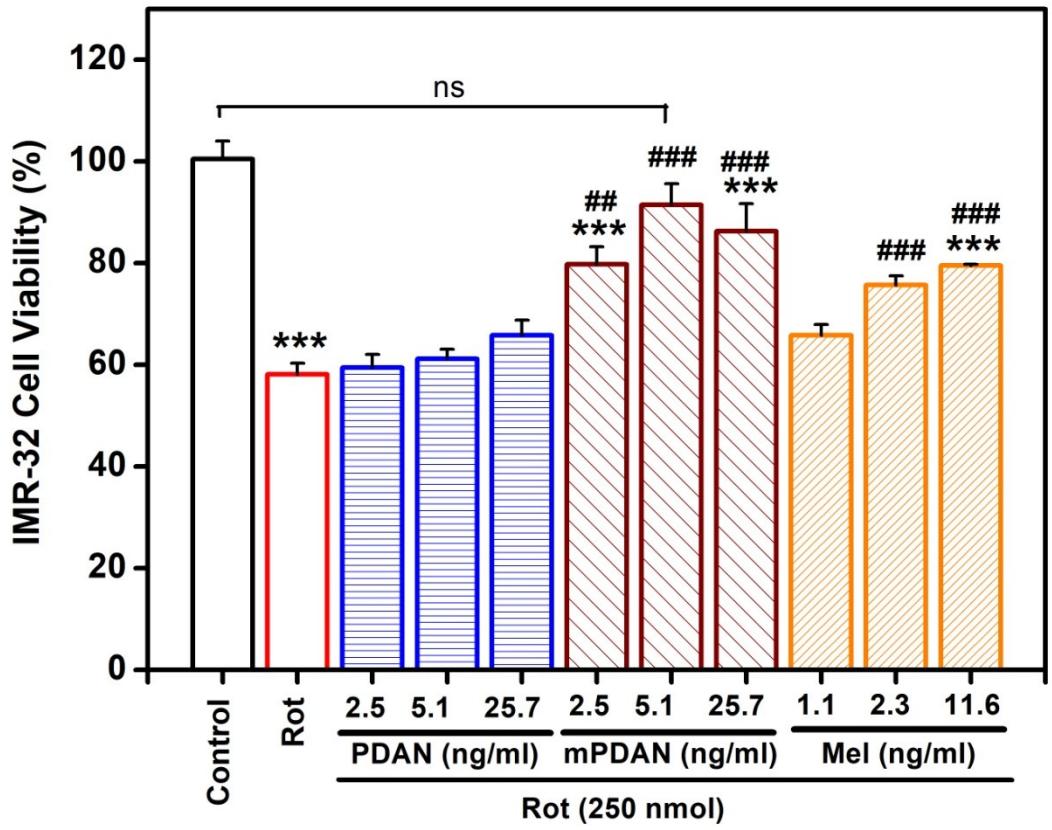

Figure S6. The 500 nM Rotenone (Rot) treatment leading 58±2% IMR-32 cell viability (Red bar) compared to untreated control considered as a model in the experiment. No significant change in the viability were obtained with co-treatment of Rot (500 nM) +PDAN (2.5 ng mL^{-1}, 5.1 ng mL^{-1} and 52.7 ng mL^{-1}) (Blue), The Rot (500 nM) + Mel (1.1 ng mL^{-1}, 2.3 ng mL^{-1} and 11.6 ng mL^{-1}) shown highest neuroprotection at 2.3 ng mL^{-1}, whereas the the Rot (500 nM) + mPDAN (2.5 ng mL^{-1}, 5.1 ng mL^{-1} and 52.7 ng mL^{-1}) represented significantly higher cell viability. The maximum cell viability (91 ±3 %) obtained for 5.1 ng mL^{-1} mPDAN were significant wrt to only Rot but not significant (ns) with respect to control. The one way ANOVA was used to compare the mean with Bonferroni significance test with respect to Control (*p≤0.05, **p≤0.01 and ***p≤0.001) and Rot (#p≤0.05, ##p≤0.01 and ###p≤0.001)

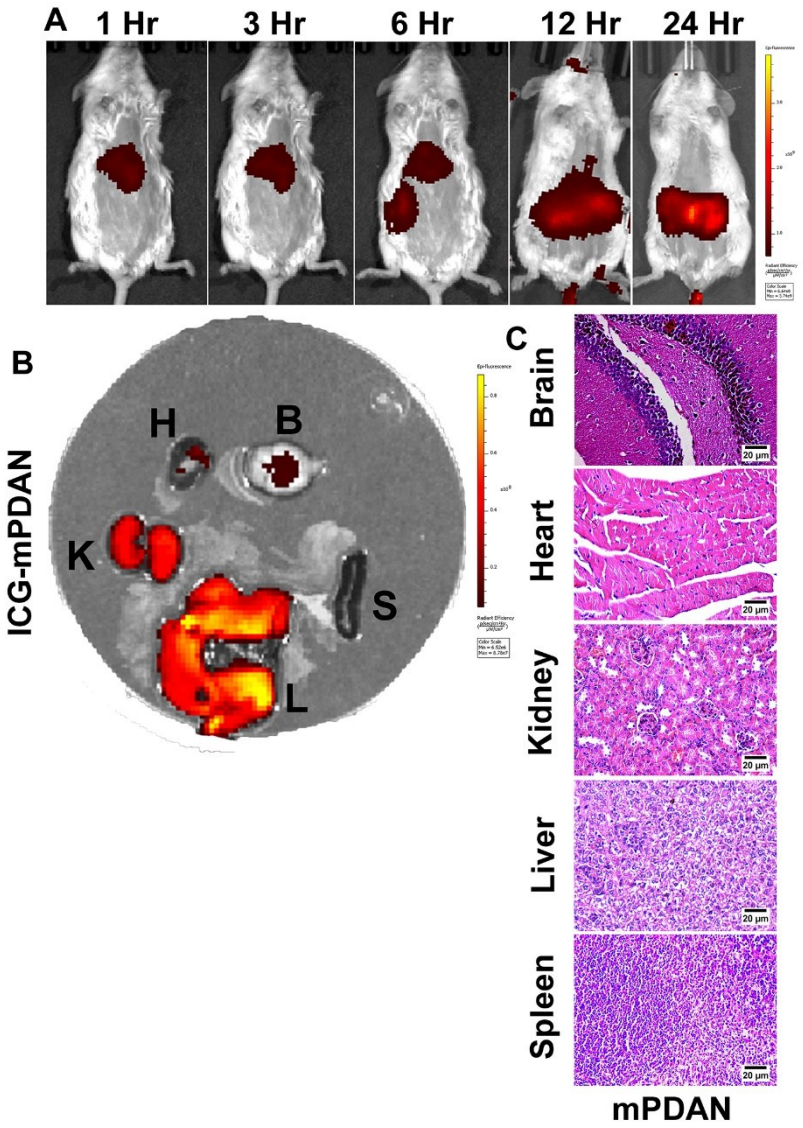

Figure S7. The *in-vivo* imaging of biodistribution and ex-vivo assessment; (A) the BALBc mice (n=4) were injected with ICG-mPDAN (1 mg kg^{-1}) via tail vein and whole-body distribution of was imaged under IVIS spectrum at different time point of 1 h, 3 h, 6 h, 12 h, and 24 h; (B) the ex-vivo imaging of the organs isolated from ICG-mPDAN treated mice showing Liver (L), Brain (B), Kidney (K), Spleen (S) and Heart (H) at 24 h post-injection; (C) Higher biocompatibility of mDPAN were concluded with

H&E histopathological staining of Liver, Kidney, Heart, Brain, and Spleen tissue section from mDPAN treated animals at 15 days post-injection (n=3). Scale bar = 20 µm

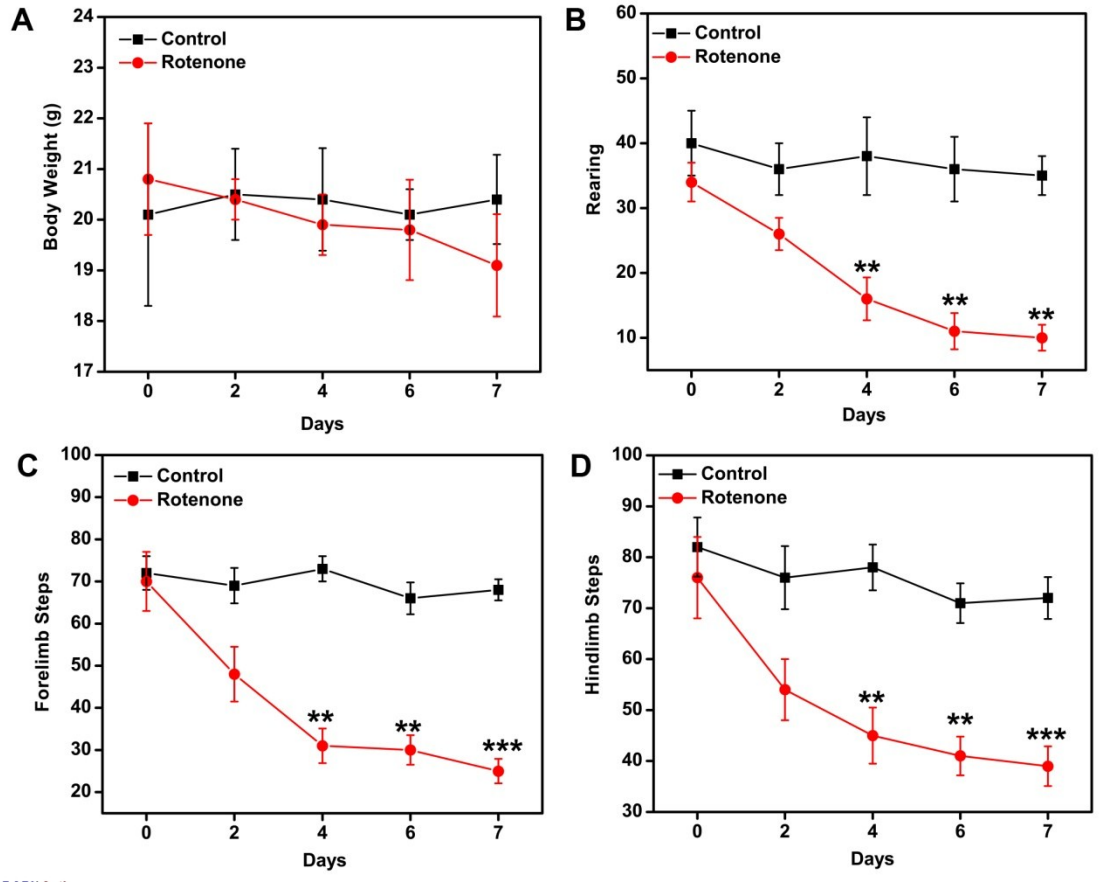

Figure S8. The behavioral studies primarily confirming the motor deficit; (A) The control and Rot injected mice were weighed before behavioral studies at 0, 2, 4, 6- and 7-day time point. The Weight difference in the control (n=12) and Rot (n=12) injected mice were significantly similar, estimated as average weight ± SEM, at *p≤ 0.05; (B) The spontaneous response in Rot injected and control mice were measured using cylinder method. The rearing, forelimb and hind limb stepping were significantly compromised in Rot injected mice at 7th day. The estimated values are

represented as Mean± SD and compared using one-way ANOVA following Tukey's significance test (*p≤0.05, **p≤0.01 and ***p≤0.001).

Table S1 Sequence information of primers using in RT-qPCR analyses

Gene (Human)	(5'-3')forward primer	(5'-3')reverse primer
Caspase-3	TTAATAAAGGTATCCATGGAGAACACT	TTAGTGATAAAAATAGAGTTCTTTTGTGAG
GAPDH	GACTCATGACCACAGTCCATGC	AGAGGCAGGGATGATGTTCTG
IL-6	CCAGCTATGAACTCCTTCTC	GCTTGTTCCTCACATCTCTC
IL-1β	AATCTGTACCTGTCCTGCGTGTT	TGGGTAATTTTTGGGATCTACACTCT
α-Syn	GCCAAGGAGGGAGTTGTGGCTGC	CTGTTGCCACACCATGCACCACTCC
PP2A	TGCTGGGGAACTCTCACTCT	TTATCGGGATCAACTCCGG
3pK	AGGCTCAAAACTTGCCTCCT	GTGTGTCCATCTATGATCCCGG
NFkB	CCCCACGAGCTTGTAGGAAAG	CCAGGTTCTGGAAACTGTGGAT